Deformation of phospholipid vesicles in an optical stretcher

Ulysse Delabre, Kasper Feld, Eleonore Crespo, Graeme Whyte, C. Sykes, Udo
Seifert, Jochen Guck

Deformation of phospholipid vesicles in an optical stretcher

Ulysse Delabre,*[abcde] Kasper Feld,[ef] Eleonore Crespo,[e] Graeme Whyte,[eg]
Cecile Sykes,[bcd] Udo Seifert[h] and Jochen Guck[ei]

Phospholipid vesicles are common model systems for cell membranes. Important aspects of the membrane function relate to its mechanical properties. Here we have investigated the deformation behaviour of phospholipid vesicles in a dual-beam laser trap, also called an optical stretcher. This study explicitly makes use of the inherent heating present in such traps to investigate the dependence of vesicle deformation on temperature. By using lasers with different wavelengths, optically induced mechanical stresses and temperature increase can be tuned fairly independently with a single setup. The phase transition temperature of vesicles can be clearly identified by an increase in deformation. In the case of no heating effects, a minimal model for drop deformation in an optical stretcher and a more specific model for vesicle deformation that takes explicitly into account the angular dependence of the optical stress are presented to account for the experimental results. Elastic constants are extracted from the fitting procedures, which agree with literature data. This study demonstrates the utility of optical stretching, which is easily combined with microfluidic delivery, for the future serial, high-throughput study of the mechanical and thermodynamic properties of phospholipid vesicles.

I Introduction

The cell membrane is a place of highly important biochemical reactions. The ability to induce and transduce biochemical signals at the cell membrane depends on its composition, organization and physical properties.[1] Vesicles composed of phospholipids are a commonly used first approach towards a realistic cell membrane.[2] Numerous studies have investigated the thermodynamic and mechanical properties of vesicles using various techniques. Among these techniques, calorimetry is the standard to study temperature transitions,[3] whereas flickering

analysis,[4] micropipette aspiration[5] or deformation of vesicles in shear flow[6,7] are approaches to characterize their mechanical properties, such as the bending modulus. Recent techniques based on the optical or electrical manipulation of vesicles have emerged that can lead to the development of microfluidic integrated systems for efficient characterization of vesicles. For example, bending moduli have been characterized by studying the deformation with optical tweezers,[8,9] or with an electric field.[10,11] However, in general, thermodynamic and mechanical characterization requires separate experimental setups which constitute a serious limit for a high throughput analysis. In the case of the optical characterization of vesicles, the choice of wavelength is crucial as heat absorption by water induces temperature changes, which can sensitively affect vesicle properties. Such temperature effects have been characterized in optical tweezers[12] and in dual-beam laser traps[13] for a specific, commonly used wavelength (1064 nm). Nevertheless, these temperature effects need not be detrimental but – if well controlled – can be usefully exploited, for example for trapping DNA.[14,15]

In this article, we study the deformation of vesicles inside a dual-beam laser trap, called an optical stretcher (OS) if used for deformation purposes,[16,17] and investigate the effect of wavelength-dependent heating on the deformation. The deformation of the vesicles in an OS is caused by optically induced surface stresses, which have been extensively used for the characterization of cell and nuclear mechanics.[17–21] While optically induced stresses are fairly insensitive to the choice of wavelength, the heat absorption of

a Univ. Bordeaux, CNRS, Laboratoire Ondes et Matière d'Aquitaine, UMR 5798, F 33400 Talence, France. E mail: ulysse.delabre@u bordeaux.fr

b Institut Curie, Centre de Recherche, Laboratoire Physico Chimie, UMR 168, F 75231 Paris, France

c Centre National de la Recherche Scientifique, UMR 168, Paris F 75231, France

d Université Paris 6, Paris F 75231, France

e Cavendish Laboratory, Department of Physics, University of Cambridge, J.J. Thomson Ave, Cambridge CB3 0HE, UK

f Niels Bohr Institute, University of Copenhagen, Blegdamsvej 17, 2100 Copenhagen, Denmark

g Institute of Biological Chemistry, Biophysics and Bioengineering, Heriot Watt University, Edinburgh, EH14 4AS, UK

h Institut fur Theoretische Physik, Universitat Stuttgart, 70550 Stuttgart, Germany

i Biotechnology Center, Technische Universitat Dresden, Tatzberg 47/49, 01307 Dresden, Germany

the medium is strongly dependent on it. This opens up the possibility of tuning the temperature optically if the wavelength is chosen correctly and controlling optically induced stress and temperature separately by the use of two appropriate laser sources. Previous studies[22–24] on the deformation of vesicles in an OS were conducted with low power 808 nm laser diodes, in which heating effects were not considered. Here, various near-infrared laser sources are used to study the influence of wavelength on the deformation and the heating of vesicles. We show (i) that a 808 nm OS can be used to study vesicle deformation without noticeable heating effects even at high power. We develop a quasispherical theory for the specific case of optical stretching to measure bending rigidity and initial tension values of the vesicles that take explicitly into account the angular dependence of the optical stress whereas previous studies were restricted to the maximum optical stress or the average optical stress exerted on the vesicle.[22–24] We then show (ii) that a 1064 nm OS can induce a significant heating of vesicles at high power and (iii) that a 1480 nm laser source can be used for intentional heating with negligible levels of optical stress induced, which can be advantageously used to probe thermodynamic properties such as the melting temperature of the phase transitions. When several wavelengths are combined together, it is then possible to manipulate optically and to control the temperature of the vesicles independently. We have developed these dual-wavelength optical stretchers both in a simple open setup configuration and in a microfluidic chamber, the latter being interesting for high throughput analysis to study the influence of drugs, pH or chemicals on membrane properties.

II Materials and methods

A Optical stretcher setups

The OS is a dual-beam optical trap that has been described in detail elsewhere.[25] Briefly, two counter-propagating laser beams, emerging from single-mode optical fibers, are combined to trap (at low power $P \leq 0.1$ W per fiber) and deform (at $P \geq 0.4$ W per fiber) vesicles using optically induced stresses. Two kinds of setups were designed for this study (see Fig. 1). The first setup called the "open setup" is more flexible and simpler to build. It is illustrated in Fig. 1d and consists in aligning the two fibers along an alignment guide (a glass capillary) fixed to a glass slide.[26] Fiber alignment was verified optically by imaging the core of the fibers in phase contrast microscopy. Of note, the open setup allows us to easily change the distance between fiber ends by pulling them apart, which in turn changes the stress profile induced on the vesicle. A micropipette was used to bring the vesicles in the center of the optical trap. A second setup called the "microfluidic setup" based on a microfluidic system, which has been described previously,[25] was used where the fiber ends are located on either side of a square glass micro-capillary (see Fig. 1e). Vesicles were injected into the glass capillary using hydrostatic reservoirs. This second setup is more complicated to build and less flexible in its operation but enables high-throughput
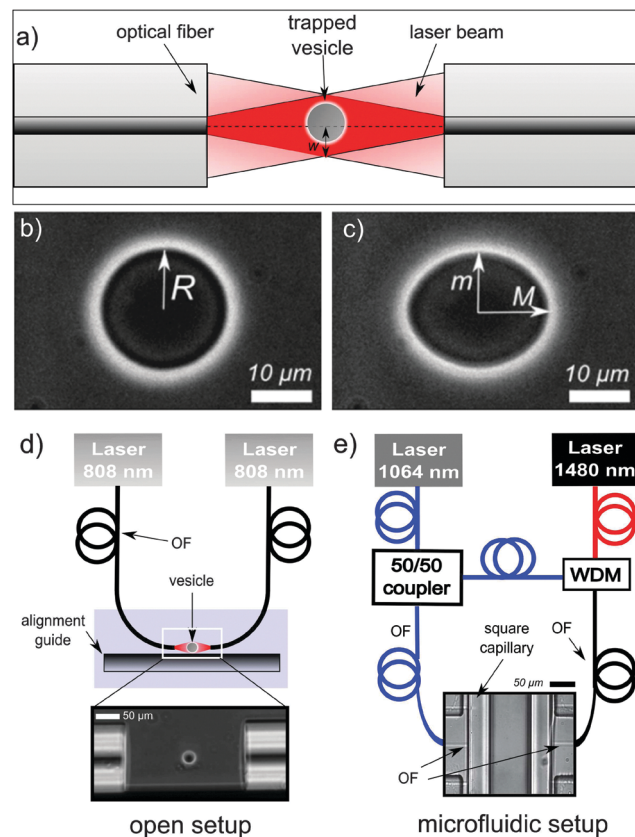

Fig. 1 (a) Sketch of the optical stretcher (OS) experiment. w is the beam radius, or beam waist, at the vesicle center. (b) Vesicle is trapped at low power ($P = 0.1$ W per fiber) and (c) deformed at high power. R is the mean radius of the undeformed vesicle; M and m are the semi major and the semi minor axis of the deformed spheroid (see the text). Here, $R = 10.6$ μm and $w = 9$ μm. (d) Sketch of the 808 nm OS arrangement in the open setup configuration. The alignment guide used in this work is a glass capillary glued to a microscope slide. (e) Sketch of the combined 1064 1480 nm lasers in the microfluidic setup. The 1064 laser is split into two optical fibers (OF) with a 50/50 coupler. One 1064 optical fiber is mixed with a 1480 laser beam with a wavelength division multiplexer (WDM). The 1064 and the 1064 1480 optical fibers are aligned perpendicular to a square micro capillary (vitrocom: I.D = 80 μm, O.D = 160 μm.)

measurements compared to the first setup as already tested for cell measurements.[25]

Different kinds of laser sources are used in this study to induce various degrees of heat absorption in the surrounding and the enclosed medium (mainly composed of water). The first laser source, an ytterbium-doped fiber laser (YLD-10-1064, IPG Photonics, Germany) operating at a wavelength of 1064 nm with a maximum power of 5 W, was used in both open and microfluidic setups. The 1064 nm laser has been the standard laser for optical stretching because the light is generated inside a single-mode fiber with sufficiently high power, turn-key operation and fast rise times (directly controlled by the current of the pump diode). The primary laser fiber was split (50:50) into two 1064 single-mode optical fibers (HI1060, Thorslabs) that are then aligned in an open setup (Fig. 1d). The second kind of laser sources were two high-power laser diodes operating at 808 nm with a maximum power of 1 W per diode (EYP-TPL-0800-01000,

Eagleyard Photonics), which were coupled into two 808 nm single-mode optical fibers (SM800-5.6-125, Thorslabs). These two optical fibers were then aligned along the capillary in an open setup. In contrast to the 1064 nm laser, the 808 nm laser option has only recently become available at the required laser powers. Light powers approaching 1 W at 808 nm are possible with a tapered diode laser, whose astigmatic output beam is coupled into a single-mode fiber, which then serves as a spatial filter and ensures a Gaussian profile of the output beam for optical stretching. This coupling requires delicate free-beam to fiber coupling using a cylindrical lens, which causes the output power to be sensitive to mechanical and thermal drift, especially when switching between low and high power operation. A feedback-controlled power adjustment reduced output power drifts and enabled the study of vesicle deformations at 808 nm with much higher powers compared to previous studies.[22–24] The third laser source, a fiber-coupled laser diode operating at 1480 nm with a maximum power of 200 mW (Alcatel 1948 PLI 200 mW, Laser 2000), was used in combination with a 1064 nm fiber with a 1064–1480 wavelength division multiplexer (Gould Fiber Optics). Light at 1480 nm is strongly absorbed by water so that this laser could be used to only heat without significant additional mechanical stress. The absorption coefficient of water at 808 nm, 1064 nm and 1480 nm is, respectively, $\alpha =$ 0.019 cm^{-1}, 0.146 cm^{-1}, and 23.239 cm^{-1},[27] which corresponds to increases in temperature of $\Delta T \approx$ 2 °C W^{-1}, 16 °C W^{-1}, and 2090 °C W^{-1} as discussed later and summed up in Table 1. To independently tune the mechanical stress and the temperature, an ideal case would be to combine 808–1480 nm sources into the same optical fiber. However, a single-mode optical fiber at 1480 nm is not single-mode for 808 nm light, which would excite higher order modes and the output beam would not be suitable for trapping and controlled deformation. Fortuitously, the single-mode fiber for 1064 nm light still permits sufficient power transmission for heating with 1480 nm light. In addition, at a given power, the heating which is directly related to the absorption coefficient is much stronger at 1480 nm than at 1064 nm. A combination of 1064–1480 sources could then be used to both deform (mainly with 1064 nm) and heat vesicles (mainly with the 1480 source). A sketch of this 1064–1480 nm laser combination is illustrated in Fig. 1e and was used in a microfluidic setup.

B Preparation of vesicles

Several types of phospholipid vesicles were prepared depending on the type of experiment. For studies at 808 nm and 1064 nm wavelengths, we use a mixture of Egg PC phospholipids (EPC), DOGS-NTA-Ni phospholipids and cholesterol (all from Avanti Polar Lipids) in a molar ratio (58 : 5 : 37) according to Pontani

et al.[28] This phospholipid mixture – called EPC for simplicity from here on – has been used to mimic cell membranes and to reconstitute actin cortices inside vesicles when combined with actin.[28] Therefore, the EPC mixture can help to understand what happens to cell membranes during optical stretching. Such EPC vesicles were used to study deformation in the 808 and 1064 nm optical stretchers. However, this EPC mixture does not have a well defined temperature transition. For thermodynamic investigation, we prepared DPPC and DSPC vesicles (Avanti Polar Lipids) to study them below and above their well-defined transition temperatures of $T_{DPPC} = 41.6$ °C and $T_{DSPC} = 55$ °C[29] in the combined 1064–1480 optical stretcher. All vesicles were prepared essentially by electroformation in a sucrose buffer solution according to the method described in ref. 23 and 30. DPPC and DSPC vesicles were grown above their melting temperature at 60 °C for DPPC and 70 °C for DSPC. Briefly, lipid mixtures were dissolved in methanol and were deposited onto ITO microscope slides and left to dry over-night. Sucrose solutions were used as an inner buffer. Vesicles were formed after 2H by applying a 1.4 V AC field at 10 Hz. Vesicles were then transferred by dilution into an outer buffer solution of glucose. In order to have a high refractive index difference that induces large optical stress, glucose and sucrose concentrations were chosen to be around 1000 mOsm of osmolarity. The refractive indexes for sucrose and glucose solutions were measured using an Abbe refractometer to be $n_{suc} =$ 1.370 and $n_{gluc} = 1.355$. To avoid any adhesion of vesicles in the microfluidic setup, this setup was previously cleaned with BSA solution. Optical stretching experiments were conducted at room temperature.

C Image analysis

Vesicles were imaged using a phase contrast microscope (Ellipse, Nikon) and recorded using a digital camera (AVT Marlin F-146B, First Sight Vision, UK). Vesicle pictures were analyzed with a custom-written Labview program. Basically, the analysis program detects the edges of the vesicle and then performs a Fourier decomposition of this 2D cross-section of the spheroidal vesicle contour. An ellipse is fitted to the Fourier contour in order to find the semi-major axis, M and the semi-minor axis m of the fitted ellipse as defined in Fig. 1c. The major axis strain (respectively minor axis strain) is defined by $\Delta M/R = (M - R)/R$ (respectively $\Delta m/R = (m - R)/R$), where R is the mean radius of the vesicle in the undeformed state.

D Calculation of optical stress and analytical approximation

The optical stretching force on a vesicle as illustrated in Fig. 2a arises from the transfer of photon momentum to the vesicle interface. Incident photons carrying a light momentum $p_{inc} = n_{med}E/c$ (n_{med} the refractive index of the surrounding medium and E the energy of the photon) are partially reflected and transmitted at the interface due to the refractive index contrast between the exterior and the interior of the vesicle. In a first analysis, the optical stress exerted at a given point of the interface is simply related to $\vec{\Delta} p = (\vec{p}_t + \vec{p}_r) - \vec{p}_{inc}$ where $\vec{p}_t$, $\vec{p}_r$ and $\vec{p}_{inc}$ are the photon momentum of the transmitted, reflected or incident photons, respectively, satisfying $p_i = n_iE/c$. However, a

Table 1 Absorption coefficients and maximum temperature increase in the setup for 1 W of total laser power for the various wavelengths used in this work

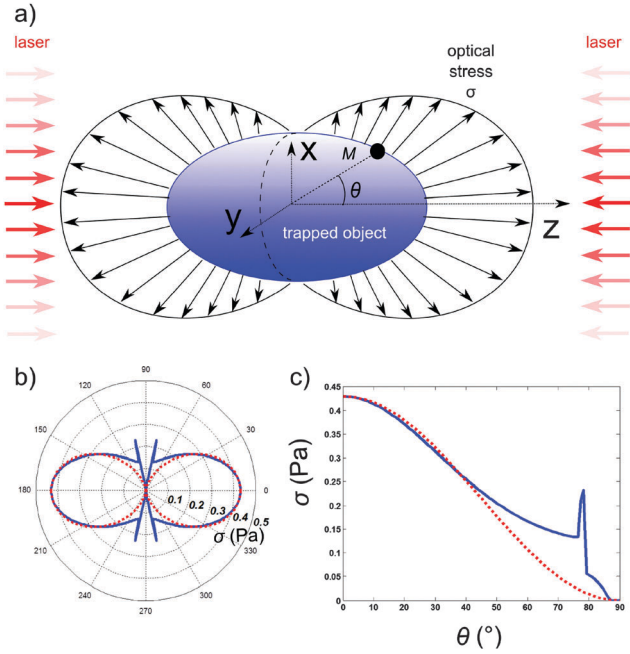| Wavelength (nm)	808	1064	1480
Absorption coefficient (cm^{-1})	0.019	0.1458	23.2394
ΔT (°C) for 1 W total power	2.3	15.9	2092.3

Fig. 2 (a) Sketch of the deformation of an object by optically induced stress (black arrows). The resulting spheroidal shape is defined by the mechanical equilibrium between surface tension, penalizing deviations from spherical shape, and optical stress, deforming the sphere along its polar axis. (b) Polar plot of a typical stress distribution obtained by RO calculation for a vesicle with radius, $R = 7$ μm, the ratio of radius to beam size, $R/w = 0.8$, a total laser power of $P = 1$ W, and the distance between the fiber end and the vesicle, $d_{\text{fiber}-\text{vesicle}} = 127$ μm ($w = 9$ μm) at 808 nm for an open setup. Stress is indicated by the concentric rings in units of Pa. The polar axis of the sphere, and later spheroid, is horizontally oriented with the laser axis. (c) Stress profile σ versus polar angle θ in a linear plot for $R/w = 0.8$. Full line shows the stress distribution from RO calculation and the dotted red line corresponds to the $\cos^2(\theta)$ approximation. Peaks at high polar angles result from specific refractions and are an artifact of the RO calculations (see the text).

full calculation of the optical stress induced on the surface of spheroidal objects is a non-trivial problem and various approximations have been proposed. The optical stress has been described using ray optics (RO) approximations with[31] or without internal reflections,[17,32] or using more exact calculations in the framework of Generalized Lorentz Mie Theory (GLMT).[33–35] The RO approximation is normally justified at a wavelength λ as long as $2\pi R/\lambda \gg 1$ and as long as the typical phase shift is such that $2\pi R(n_{\text{scat}}/n_{\text{med}} - 1)/\lambda \gg 1$,[36] where n_{scat} and n_{med} represent the refractive index of the scatterer and the medium, respectively. For our experiments, vesicles where chosen with $R \geq 4$ μm implying that the first condition is well fulfilled since we used light with wavelengths between 0.808 μm and 1.5 μm. The second condition seems to be more difficult to satisfy for biological samples as $\Delta n = (n_{\text{scat}} - n_{\text{med}}) \leq 0.04$ and $n_{\text{med}} \approx 1.33$–$1.35$, which implies $R \gg 8$ μm. In this study, radii were between 4 μm and 13.5 μm. However, the accuracy of RO approximations has recently been compared to GLMT calculations.[34] Interestingly, the RO approximation can well describe the stress within 10% even in the case where the phase shift is only close to one ($2\pi R(n_{\text{scat}}/n_{\text{med}} - 1)/\lambda \approx 0.8$). The main discrepancy between RO and GLMT occurs at the equator of a spheroid oriented along the laser axis, where the RO approximation

assumes a zero electromagnetic field, which is not the case. Therefore, in the present work the optical stress was calculated using RO. In addition, during stretching the vesicle is deformed and the distribution of optical stress induced at its surface might change. This question has been recently addressed with more elaborate numerical methods that take into account the spheroidally deformed shape.[34] It has been shown that the peak stress – *i.e.* the maximum stress – and stress distributions are similar within 10% between the elongated spheroid and the sphere as long as relative axial deformations remain below 10%. Therefore, we have neglected this small change and considered that the stress profile for both spherical and spheroidal vesicle is sufficiently well described by the stress applied on the spherical shape. Thus, in this work the optically induced stress is numerically computed for the initial spherical shape based on RO approximations as described in ref. 32. Because the refractive index contrast is small ($\Delta n \leq 0.015$), multiple reflections could be neglected as in ref. 17 as they do not contribute significantly to the stress. Typical stress profiles are shown in Fig. 2b and c. The peak stress σ_0 is obviously along the fiber axis and can be related to refractive indexes and beam intensity by a simple formula given in the ESI.† As in other RO studies,[31,32] peaks at a high polar angle ($\theta \approx 80°$) appear. They constitute an artifact of the RO approach[34] due to specific refractions inside the vesicle as well described in ref. 32. Such peaks do not contribute significantly to the total stretching force – defined as the projection of the total optical force along the fiber axis – since these peaks are very localized. Fig. S2 (see ESI†) shows that the optical stress profile depends on the ratio R/w between the radius R of the vesicle and the beam waist w at the vesicle center. Basically, when $R/w \leq 1$, the entire vesicle is exposed to laser beams, which leads to an almost homogeneous optical stress, whereas for $R/w > 1$ the optical stress profile is more localized. Previous studies have considered either a mean optical stress[22] or the maximum stress[23] to describe the deformation of vesicles. However, the optical stress profile and thus the total projected stretching force (as shown in Fig. S2 (see ESI†)) strongly depend on the ratio R/w. In this work, we develop a quasispherical approach to characterize vesicle deformation with the optical stretcher that takes into account the angular dependence of the optical stress profile. As no exact analytical expression of the optical stress exists, we use a $\cos^2$ approximation as motivated in ref. 17 and 38 and defined by $\sigma(\theta) = \sigma_0 \cos^2 \theta$ where σ_0 is the peak stress obtained from RO calculations. Interestingly, such an approximation has proved to work relatively well when $R/w \approx 0.8$–0.9 as shown in Fig. 2b. This specific profile will constitute the basis for the analytical treatment of vesicle shape deformations as presented below but other analytical approximations could be adapted in future studies.

III Theory: deformation in the optical stretcher

A Minimal model for deformation of a liquid drop in an optical stretcher

Vesicles are often described as very soft objects with very low tension.[39] So, a first approximation considers the vesicle as a

liquid drop with isotropic properties and a constant surface tension, Σ_0. This liquid drop model follows the approach developed in ref. 40 for optical tweezers and extends it for the specific case of the OS where the locally varying stress profile has to be taken into account and not only a total deformation force. Such a simple model can provide a useful comparison between vesicle and drop deformations.

Locally, the law of Laplace for a polar angle θ can be written according to the geometry defined in Fig. 2a as:

$$\Pi_{\text{int}} \quad \Pi_{\text{ext}} + \sigma(\theta) = \Sigma_0 C(\theta), \tag{1}$$

where Π_{int} and Π_{ext} are the internal and external pressure, $\sigma(\theta)$ the local optical stress, and C the local curvature. Note that since the problem is rotationally symmetric with respect to the fiber axis, the azimuthal angle ϕ does not appear in the equations and only the polar angle θ has to be taken into account. Subtracting the two equations for polar angles of θ and $\theta = \dfrac{\pi}{2}$ allows the elimination of the pressure difference, and yields

$$\sigma(\theta) \quad \sigma\left(\frac{\pi}{2}\right) = \Sigma_0 \left(C(\theta) \quad C\left(\frac{\pi}{2}\right) \right). \tag{2}$$

Integrating this relation projected along the fiber axis gives the equilibrium between the optically induced axial deformation force and the restoring force due to surface tension:

$$\int_0^{\frac{\pi}{2}} \left(\sigma(\theta) \quad \sigma\left(\frac{\pi}{2}\right) \right) \mathrm{d}S = \int_0^{\frac{\pi}{2}} \Sigma_0 \left(C(\theta) \quad C\left(\frac{\pi}{2}\right) \right) \mathrm{d}S, \tag{3}$$

The vesicle is assumed to be deformed into a prolate shape and is characterized by the semi-major axis M and the semi-minor axis m. Volume conservation implies $\Delta M = 2\Delta m$. So, $m = R(1 \quad \Delta M/(2R))$ and $M = R(1 + \Delta M/R)$ to first order in $\Delta M/R$.

The local curvature at angle θ is the curvature of the associated prolate:

$$C(\theta) = \frac{M\left(m^2 + M^2 + \left(m^2 \quad M^2\right)\cos^2\theta\right)}{m\left(M^2 + \left(m^2 \quad M^2\right)\cos^2\theta\right)^{3/2}}, \tag{4}$$

thus the right hand side of eqn (3), *i.e.* the global restoring force on one half of the droplet along the fiber axis due to surface tension can be expressed to first order in $\dfrac{\Delta M}{R}$ as

$$3\pi R \Sigma_0 \left(\frac{\Delta M}{R} \right) \vec{e}_z, \tag{5}$$

which is equivalent to the expression in ref. 40. To introduce the optically induced force, we use the *ad hoc* approximation of the stress profile as $\cos^2(\theta)$ for the further first-order, analytical derivation of the deformation, which yields for the left hand side of eqn (3)

$$\frac{\pi R^2 \sigma_0}{2} \vec{e}_z. \tag{6}$$

The final deformation $\dfrac{\Delta M}{R}$ is given by mechanical equilibrium between these two forces, from which we get a very simple relation between the deformation for small stress and small deformation $\left(\dfrac{\Delta M}{R} \ll 1 \right)$

$$\frac{\Delta M}{R} = \frac{\sigma_0 R}{6\Sigma_0}. \tag{7}$$

This minimal model does not take into account the bending energy and the possible dependence of the tension on the applied stress as it should be the case for a vesicle. In the next section, a quasi-spherical approach is developed to describe the specific case of vesicles more appropriately.

B Deformation of a vesicle in the optical stretcher

We analyze the deformation of a vesicle according to the quasi-spherical approach described in ref. 41 and 42. In this approach, the shape of the vesicle is parametrized in spherical harmonics as

$$R(\theta, \phi) = R \quad 1 + \sum_{l \geq 0}^{l_{\max}} \sum_{m \quad -l}^{l} u_{lm} \mathcal{Y}_{lm}(\theta, \phi) \Bigg), \tag{8}$$

where $\mathcal{Y}_{lm}(\theta, \phi)$ are the normalized spherical harmonic functions and u_{lm} their associated amplitudes. The radius of the vesicle R is given by the constant volume of the vesicle as $V = \dfrac{4\pi R^3}{3}$. We assume that the total area A of the vesicle is fixed and can be expressed by $A = (4\pi + \Delta)R^2$ where Δ is the dimensionless excess area related to the difference between apparent area and true area. Below, we only summarize the important equations and results of this approach. A full description is available in the ESI.†

The energy induced by the optical stretcher is taken into account in the total free energy of the vesicle. Basically, the optical stretcher will deform the vesicle and pull membrane fluctuations. The shape of the vesicle results then from the minimization of the free energy. The total free energy is the sum of three terms: the bending energy F_κ, a surface energy F_Σ and the deformation or "stretching" energy F_s as

$$F = F_\kappa + F_s + F_\Sigma. \tag{9}$$

The area constraint is taken into account as an area energy such that

$$F_\Sigma = \Sigma \oint \mathrm{d}A, \tag{10}$$

where the effective tension Σ of the vesicle is the Lagrangian multiplier associated with the area. We define a dimensionless tension $\tilde{\gamma}$ by $\tilde{\gamma} \equiv \Sigma R^2/\kappa$.

To model the deformation energy, we use the analytical approximation suggested by Wottawah *et al.*[37] where the stress is approximated by $\sigma(\theta) = \sigma_0 \cos^2(\theta)$. The calculation below can be extended to other analytical functions for the stress as it is always possible to decompose the stress distribution in spherical

harmonics and do a similar development as below. Thus, in the case of $\sigma = \sigma_0 \cos^2(\theta)$, the deformation energy is

$$F_s = \sigma_0 \oint \cos^2\theta[R(\theta,\phi) \quad R]\mathrm{d}A \qquad (11)$$

The stress distribution can be decomposed in spherical harmonics to give $\cos^2(\theta) = \left[\sqrt{16\pi/5}\mathcal{Y}_{20} + 1\right]/3$. So the deformation energy becomes

$$F_s = (\sigma_0 R^3/3)\left[\sqrt{4\pi}u_{00} + \sqrt{16\pi/5}u_{20}\right]. \qquad (12)$$

By defining $\tilde{f} = \dfrac{2\sigma_0 R^3}{3\kappa}$ as a dimensionless stress parameter, the expression of the total free energy is

$$F = \frac{\kappa}{2}\sum_{l,m} E_l|u_{lm}|^2 \quad \kappa\tilde{f}\sqrt{4\pi/5}u_{20}, \qquad (13)$$

with

$$E_l = (l+2)(l \quad 1)[l(l+1) + \tilde{\gamma} + \tilde{f}/(l+2)(l \quad 1)]. \qquad (14)$$

The mean shape of vesicles in the optical stretcher now follows from this energy as there is only one mode with a non-zero mean amplitude which is the elliptical one,

$$u_{20} = \frac{\sqrt{4\pi/5}\tilde{f}}{24 + 4\tilde{\gamma} + \tilde{f}}, \qquad (15)$$

where the bar on any parameter indicates the change due to the optical stretcher related to the spherical case. Experimentally, $\bar{u}_{20}$ is directly related by eqn (8) to the relative major and minor axis strains, ΔM and Δm, respectively, by

$$u_{20} = \frac{2}{3}\sqrt{\frac{4\pi}{5}}\left(\frac{\Delta M}{R} \quad \frac{\Delta m}{R}\right). \qquad (16)$$

The area stored in the elliptical mode is, from eqn (15) and area constraint

$$\Delta = 2u_{20}^2 = 2\frac{(4\pi/5)\tilde{f}^2}{(24 + 4\tilde{\gamma} + \tilde{f})^2}. \qquad (17)$$

By defining Δ_{fl} the area stored in fluctuation which can be expressed explicitly (see ESI†), the total area constraint reads then

$$\Delta = \Delta + \Delta_{\mathrm{fl}}. \qquad (18)$$

This equation is the general equation to calculate the dependence of the effective tension $\tilde{\gamma} = \tilde{\gamma}(\Delta, \kappa, \tilde{f}, l_{\max})$ and to deduce the vesicle shape in the optical stretcher.

For vanishing laser amplitude ($\tilde{f} = 0$) the dimensionless initial effective tension $\tilde{\gamma}_0 = \dfrac{\Sigma_0 \cdot R^2}{\kappa}$ (resp. the initial effective tension Σ_0) can be derived analytically from eqn (18) in three regimes[41] as described in the ESI.† In this work we are mainly interested in the entropic regime, which corresponds to low effective tensions between $10^{-7} \ll \Sigma_0 \ll 10^{-3}$ N m^{-1} for $\kappa \approx$ 1–100kT and $R \approx 10$ μm.

For low laser power, the applied stress is weak and the tension term is dominant if $4\tilde{\gamma} \gg \tilde{f}$ in eqn (15) and (17). This condition is fulfilled in our experiment at small power (see the experimental part). In this low peak stress regime ($\sigma_0 R \ll 6\Sigma$), we can then obtain a simple expression for the deformation $\bar{u}_{20}$

$$u_{20} \approx \frac{\sqrt{4\pi/5}\tilde{f}}{24 + 4\tilde{\gamma}}, \qquad (19)$$

where $\tilde{\gamma}$ is the effective tension of the vesicle that depends implicitly on the stress but should be close to the initial tension $\tilde{\gamma}_0$ as calculated above.

Finally, the mean shape of the vesicle in the optical stretcher is given by

$$\langle R(\theta,\phi)\rangle = \tilde{R} + Ru_{20}\mathcal{Y}_{20}, \qquad (20)$$

where $\tilde{R} = R\left(1 + \langle u_{0,0}\rangle/\sqrt{4\pi}\right)$.

Considering that in first order, $\tilde{R} \approx \tilde{R}(0) + B\cdot\tilde{f}$, the mean shape of the vesicle in first order becomes

$$\langle R(\theta,\phi)\rangle \approx \tilde{R}(0) + \left[B + \frac{R}{24 + 4\tilde{\gamma}}(3\cos^2\theta \quad 1)/2\right]\tilde{f}, \qquad (21)$$

where $\tilde{R}(0)$ is the mean radius at zero optical stress and B is a term independent of $\tilde{f}$.

To take into account the total area constraint (eqn (18)), we can simplify area expressions using the low peak stress approximation for the entropic regime, which gives

$$\Delta = \frac{kT}{2\kappa}\ln\left(\frac{\Sigma}{\Sigma_0}\right) = \frac{kT}{2\kappa}\ln\left(\frac{\tilde{\gamma}}{\tilde{\gamma}_0}\right), \qquad (22)$$

where Σ_0 and Σ are the vesicle effective tension (in N m^{-1}) for the initial spherical case and the deformed case. This relation is similar to the one developed in ref. 6, noticing that $\Delta A/A = \Delta/4\pi$. However, the effective tension cannot be rigorously determined by the law of Laplace as presented for the minimal liquid drop model, since fluctuations and bending rigidity modify it.[43] But by combining eqn (17) and (22), we can eliminate the effective tension of the vesicle in eqn (19) and obtain a relation between $\bar{u}_{20}$ and the peak stress σ_0 within this approximation

$$\sigma_0 = \sqrt{\frac{5}{4\pi}}u_{20}\left(\frac{36\kappa}{R^3} + \frac{6\Sigma_0}{R}\exp\left(\frac{4\kappa u_{20}^2}{kT}\right)\right), \qquad (23)$$

where the fitting parameters are κ and Σ_0, respectively, the bending modulus and the effective initial tension of the vesicle. Eqn (23) is the standard equation that will be tested where $\bar{u}_{20}$ is evaluated experimentally (with eqn (16)) and the peak stress σ_0 calculated numerically from experimental parameters.

It is worth noticing that when bending modulus is set to $\kappa = 0$ in eqn (23), we find again eqn (7) of the minimal model using eqn (16). Furthermore, the above theoretical description is valid as long as $\sigma_0 R \ll 6\Sigma$ (i.e. $4\tilde{\gamma} \gg \tilde{f}$). When the stress is increased and becomes large enough ($\tilde{f} \rightarrow \infty$), the above approximation breaks down and all the excess area will be stored in the elliptical mode $l = 2$. The tension in the vesicle, which depends on the applied stress, is also increased and is expected to depend linearly on the peak-stress in the high peak stress regime (see ESI†). Above a critical stress σ_c, the deformation

of the vesicle is expected to saturate with $u_{20} \to \sqrt{\frac{\Delta}{2}}$ as long as the quasispherical approach is still appropriate. Indeed, in the high peak stress regime, stronger deformations could take place and further effects such as stretching (*i.e.* dilatation) of the membrane might arise which are not studied here.

IV Experiments

A Deformation of vesicles with an 808 nm optical stretcher

EPC vesicles were deformed with the 808 nm open setup. Vesicles were trapped at relatively low power ($P \approx 0.1$ W per fiber). We first performed some step-stress tests, where the power was rapidly increased from the trap power to a given stretching power and then maintained for 4 s before reducing back to trap power. A typical vesicle deformation characterized by the major axis strain $\Delta M/R = (M - R)/R$, for a step-stress test, is shown in Fig. 3a. It appears that vesicles respond very quickly to the applied stress as they rapidly reach their final deformation and go back to their initial shape, especially compared to cells.[37]

As explained in the Methods section, the laser-fiber coupling was delicate for the 808 nm laser, especially when going from trap power to high power, and a transition time was required to reach the selected power. In order to minimize this transient effect, the power was increased by 0.05 W per fiber step-by-step from the trap power and was kept constant for 15 s to record the steady-state shape of the vesicle. After 15 s, the power was then increased to the next step up to the maximum power ($P_{\max} \approx 0.6$ W per fiber). A typical step-by-step deformation is shown in Fig. 3b where the major axis strain $\Delta M/R$ and minor axis strain $\Delta m/R$ of the fitted ellipse are plotted *versus* total power. Data can be well described by linear fits. The volume conservation of the spheroids implies that $\Delta m/R = -2\Delta M/R$ which is verified experimentally within the uncertainty of the data (see Fig. 3c). In addition,

in Fig. 3b, two sets of data are shown that correspond to two series for the same vesicle from the trap power to the maximum power. The second set of data shows an identical trend indicating that no hysteresis exists for vesicles stretched by a 808 nm optical stretcher, *i.e.*, with very low laser heating, even at high power (total power $P \sim 1$ W).

We deformed several vesicles with different ratio R/w at a fixed fiber distance ($d_{\text{fiber–fiber}} = 254$ µm), where R is the mean radius of the vesicle and w is the beam radius at the vesicle position. In the experiment, fiber distance, and so beam waist $w (w \approx 9$ µm), were kept constant whereas various vesicles with different radii were investigated. To test the minimal model of eqn (7), deformation data *versus* the peak stress σ_0 are plotted in Fig. 4 and rescaled *versus* $\sigma_0 R$. Clearly, the data are well rescaled by this simple model even if some discrepancies seem to exist for small ratio R/w. The fitted slope found is 0.038 Pa^{-1}. µm^{-1} which corresponds to initial effective vesicle tensions around $\Sigma_0 = (4.3 \pm 0.5) \times 10^{-6}$ N m^{-1}. However, we do not expect this model to describe vesicle deformations perfectly as it is not adequate to fit all vesicle data with the same initial tension Σ_0. Furthermore, the vesicle tension is not constant but increases with the applied stress as described in the quasi-spherical approach. The relatively good agreement of the rescaling seems to indicate that vesicle tensions do not vary so much in our case from the value $\Sigma_0 = 4.3 \times 10^{-6}$ N m^{-1}, which is in agreement with values of initial tensions of floppy vesicles reported in the literature.[10] This would suggest that the low peak-stress regime is applicable here.

To extract bending rigidity values, we have tested the model based on the quasi-spherical approach presented in eqn (23). Results are reported in Fig. 5 where the peak-stress σ_0 calculated from RO is plotted *versus* $\bar{u}_{20}$ estimated from eqn (16). In the low peak-stress regime of deformation, the term associated with tension is dominant if $\Sigma \gg \frac{\sigma_0 R}{6}$. With a vesicle radius on the order of $R \approx 10$ µm and $\Sigma \approx 4 \times 10^{-6}$ N m^{-1}, the low peak-stress
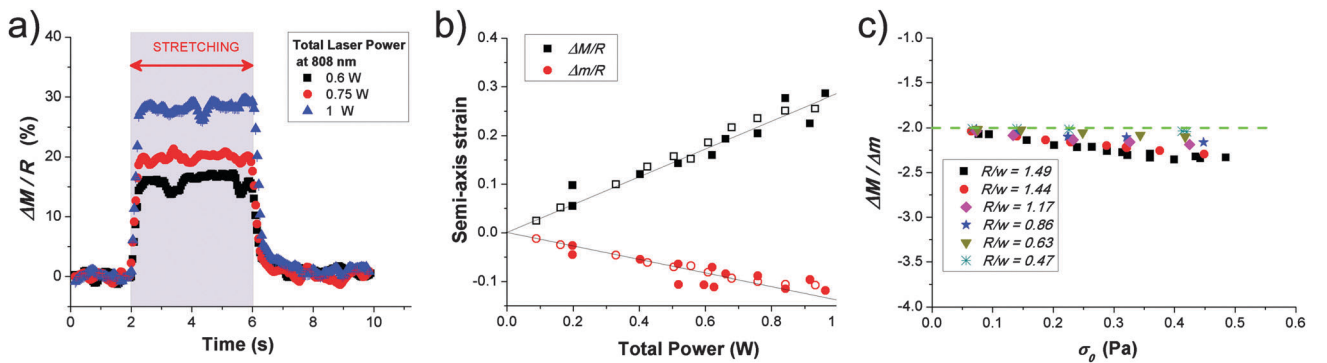

Fig. 3 (a) Deformation of a vesicle with the 808 nm open setup. The major axis strain, $\Delta M/R$, is shown as a function of time for a 4 s stretch at various total powers for the two fibers as indicated in the legend (P = 0.6 W, 0.75 W or 1 W). The vesicle is trapped at low power ($P \approx 0.1$ W) between 0 – 2 s. The stretch power is applied between 2 – 6 s. (b) Major axis strain and minor axis strain as a function of the applied power. Squares (black) represent the major axis strain and circles (red) represent the minor axis strain. Filled symbols are for the first series of measurements. Open symbols are for the second series. Solid lines are linear fits with a slope of 0.285 ± 0.018 W^{-1} for the major axis strain and -0.122 ± 0.018 W^{-1} for the minor axis strain. (c) Ratio between major and minor axis strains as a function of peak stress, σ_0, for different ratios R/w (R is the radius of the vesicle and w is the waist of the beam at the vesicle position). The ratio $\frac{\Delta M}{\Delta m}$ is close to the theoretical limit -2 corresponding to volume conservation of a spheroid.
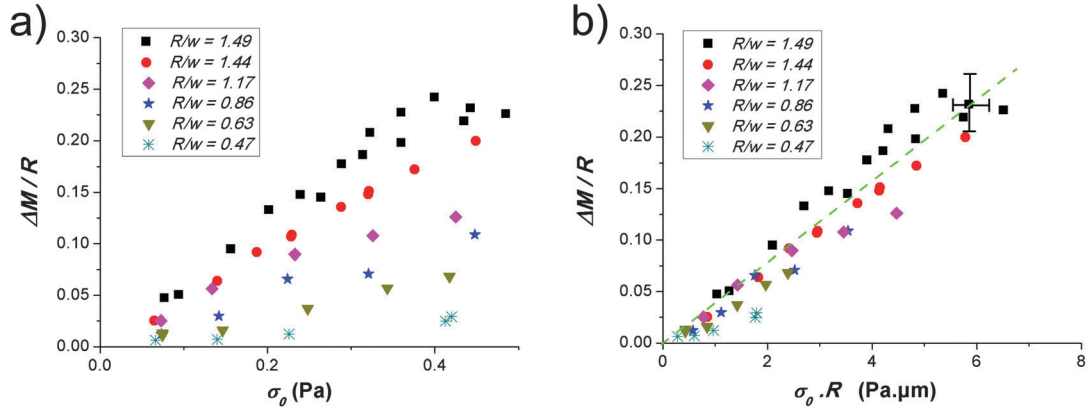
Fig. 4 (a) Deformation of 808 nm data characterized by the major axis strain $\Delta M/R$ versus the calculated peak stress for various ratios R/w. (b) Rescaled data according to the model presented in eqn (7). A typical error bar is indicated and similar error bars exist for other data points but are not shown for clarity.
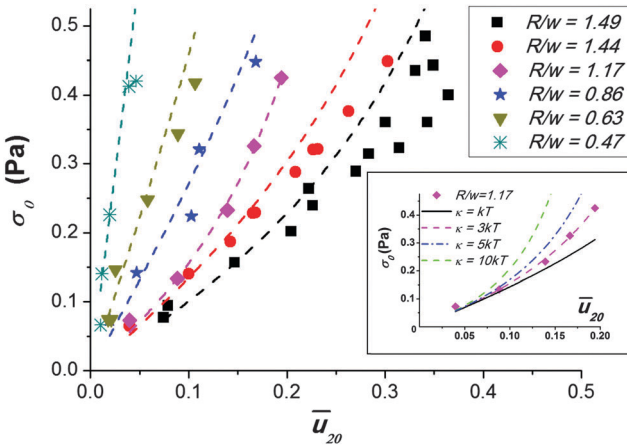

Fig. 5 Comparison between experimental data for the deformation of vesicles with the 808 nm setup with the quasispherical model of eqn (23). Beam waist is $w \approx 9$ μm. Bending modulus κ and initial tension of vesicles are extracted from the fitting procedure. The mean fitting values are for bending modulus $\kappa = 2.5kT$ and initial tension values Σ_0 are between 3 – 7.5×10^{-6} N m^{-1}. Insert: example of the effect of the bending modulus on the fit for $R/w = 1.17$. The best fit corresponds to $\kappa = 3kT$ and an initial tension $\Sigma_0 = 3.85 \times 10^{-6}$ N m^{-1}. Other curves correspond to different bending modulus values and the same initial tension $\Sigma_0 = 3.85 \times 10^{-6}$ N m^{-1}. Bending modulus is from the bottom to the top $\kappa = 1kT$; $3kT$; $5kT$; $10kT$.

regime is applicable, if the peak stress σ_0 is $\ll 2.5$ Pa, which represents an important part of the stress range applicable with the available 808 nm laser. The model has been fitted for bending moduli between 1–$100kT$. The fitted values of bending moduli are between 1–$7.5kT$, with a mean value of $2.5kT$ whereas the fitting values for Σ_0 are between 3–7.5×10^{-6} N m^{-1} close to the value found earlier with the minimal model of eqn (7). An example of the sensitivity of the model to fitting parameter is shown in the inset of Fig. 5. Most of the previously reported values for κ for EPC vesicles have been around $6.18kT$[10] and 10–$11kT$[48] even if some higher values of the bending moduli have been reported ($57kT$[47]). The values obtained here are then slightly lower than the values reported in the literature. This may indicate that the simple $\cos^2$ approximation is not appropriate to fully describe the shape of

vesicles in the optical stretcher, as discussed later. Another possible explanation might be the high osmolarity of solutions used here to increase the refractive index contrast. It has been reported that the bending modulus tends to decrease with the osmolarity,[23,50] which could explain the smaller values obtained here. It is also important to verify that dilatation of the membrane area is negligible in our experiments. Using the fitted values of κ and Σ_0 for each vesicle in eqn (22), it is possible to calculate their effective tension Σ during deformation. We obtained effective tension values which are less than 5 times their initial tension Σ_0. Considering that the area expansion modulus is $K_a \sim 200$ mN m^{-1},[5,49] the increase in membrane surface area due to dilatation can be estimated with the following equation $(\Delta A/A)_{\text{dilatation}} = (\Sigma - \Sigma_0)/K_a$. At most, the increase in membrane surface area due to dilatation is found to be 2% of the increase due to the fluctuations which confirms that our data have been taken entirely in the entropic regime. It can also be surprising that the minimal model presented for a liquid drop works relatively well. However, to understand this, it is sufficient to evaluate each term in $\bar{u}_{20}$ of eqn (15). In the low peak stress regime, which represents an important range of our data, the tension term is dominant in the expression of $\bar{u}_{20}$ since $4\tilde{\gamma} \gg \tilde{f}$. In addition it is easy to verify that $4\tilde{\gamma} \gg 24$, with $\kappa \approx 1$–$10kT$. Thus, when this approximation is valid, the expression of $\bar{u}_{20}$ can be simplified to

$$u_{20} \approx \frac{\tilde{f}}{4\tilde{\gamma}}.$$ With eqn (16) and $\Delta M/R = -2\Delta m/R$, we find again the

equation of the minimal model: $\Delta M/R = \dfrac{\sigma_0 \cdot R}{6\Sigma}$. This simplified calculation explains also why the saturation regime is not present in the 808 nm deformation data since the peak stress is too small to satisfy $\sigma_0 \gg \sigma_c$ (see ESI†) since $\sigma_c \approx 1$ Pa with $\Sigma_0 \approx 10^{-6}$ N m^{-1} and $R \approx 10$ μm. To reach this saturation regime, the use of smaller initial tension or higher power at 808 nm might help in future studies once appropriate laser sources become available.

B Deformation of vesicles with an optical stretcher at 1064 nm

In this section, we describe the deformation of vesicles with an optical stretcher operated at 1064 nm, which, in addition to

deforming the vesicle, induces significantly more heating than at 808 nm. Similar EPC vesicles were deformed with an open 1064 nm setup which can go to higher stretching powers (P_{max} = 2.5 W per fiber compared to 0.6 W per fiber at 808 nm). A first important difference at 1064 nm with the deformation at 808 nm is shown in Fig. 6a, where the major axis strain changes during the stretching which was not the case for 808 nm stretching (compare with Fig. 3a). The deformation increases rapidly after the application of the stretching power but starts to decrease during the application of the stretching power. Experimentally, we did not loose contrast, which allows us to rule out a possible formation of a pore or a lysis of the vesicle and which could have led to a decrease in the refractive index contrast and thus applied stress. Using optical tweezers, Bar-Ziv et al.[46] have shown that a strongly focused laser beam could locally induce a high tension comparable to the tension needed to induce packing of lipids and buckling of the bilayers which tends to reduce true membrane area. With optical stretchers, the laser beams are not focused and the divergence of the beams enables us to avoid strong intensity gradients and such a reshaping of the lipid bilayer. Furthermore, such a decrease in deformation does not exist with the 808 optical stretcher, which suggests that this effect can be attributed to the heating induced by laser absorption. Indeed Ebert et al.[13] have reported that the temperature increase in the optical stretcher for 1064 nm is about 13–17 °C W^{-1} (total power) whereas it is negligible (1.7 °C W^{-1}) for 808 nm. The temperature rise in the setup is almost instantaneous according to Ebert et al.[13] (typically a few ms), which matches the experimental observation that the deformation starts to decrease as soon as the stretching power is applied. The example of deformation shown in Fig. 6a and b clearly indicates that the rate of decrease in the major axis strain increases with the power applied during stretching. The implication of heating as the likely cause of this phenomenon is also supported experimentally by the observation of enhanced fluctuations for some vesicles during the stretching time especially for high power. Heating by 1064 nm light might also induce some phase transitions and

reorganization during the stretching. Indeed, in EPC vesicles, various lipids might transit over their phase transition temperature such as ((16 : 0) (T = 41 °C) or (17 : 0) (T = 48 °C)) lipids. In addition, the cholesterol could also strongly modify the phase diagram of the lipid mixture.[44,45] This strain decrease was observed for most of the vesicles and could result in a significant hysteresis of the deformation. Indeed, a second stretch at the same power could show a completely different deformation (not shown). This suggests that an irreversible change in the membrane organization could have occurred. We also note that some of the vesicles do not exhibit a decrease in the deformation during stretching but an increase. Such a strain decrease and hysteresis in deformation might also be the signature of hidden area or defects that are pulled out or created with temperature as it has been reported in micro-pipette manipulation studies for example.[44] However, this hysteresis does not exist in the 808 nm deformation data which supports the idea that the temperature increase triggers a possible microscopic reorganization of the membrane. These effects make the deformation of vesicles difficult to analyze and seem to be specific to each vesicle. We nevertheless report the major axis strain (Fig. 6c) for some vesicles where values were taken at the beginning of the stretching time (t = 2 s) i.e. where the deformation is maximum in Fig. 6a. The power was increased step-by-step from low power to high power to keep hysteresis effects to a minimum. Interestingly, the increase in deformation is higher for low peak stress than for high peak stress which was not the case for the 808 nm open setup (see Fig. 4a). A saturation is predicted by the model described in the ESI† for sufficiently high peak stress $\sigma_0 > \sigma_c$ but the additional influence of heating makes it difficult to quantitatively analyze this saturation behaviour in the current theoretical framework.

C Deformation of vesicles with a combined optical stretcher at 1064/1480 nm

To further investigate the variation of deformation with temperature and to test the ability of dual-beam optical traps to combine stretching and heating, we use a wavelength-division
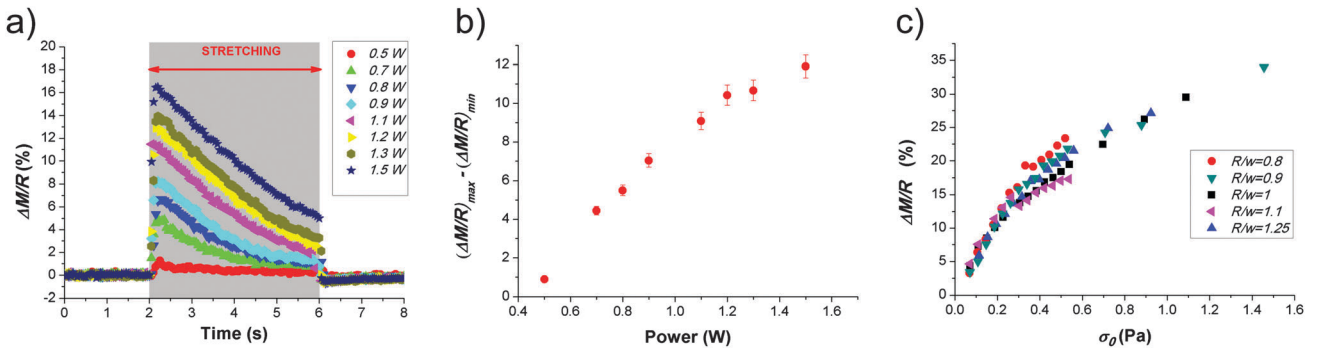

Fig. 6 Vesicle deformations with concurrent heating. (a) Major axis strain (in%) of a vesicle (R/w = 1.22) deformed with laser light at 1064 nm. The continuous decrease in strain during constantly applied optical stress is associated with heating effects (see text). From absorption coefficients presented in Table 1, maximum temperature increases are expected to range linearly from 8 °C to 24 °C above the room temperature for the investigated powers. (b) Difference between the relative major axis strain at t = 2 s (maximum extension) and t = 6 s (minimum extension). (c) Maximum of the major axis strain versus maximum optical stress for different vesicles.

multiplexer to add the output of a single-mode fiber-coupled diode laser operating at 1480 nm wavelength to one of the two optical stretcher fibers, which carry light at 1064 nm wavelength as presented in the Materials section. Furthermore, as detailed below, it enables us to mainly control the optical stress with the 1064 nm and to mainly control temperature with the 1480 nm laser. The two fibers forming the optical trap (one: 1064 nm; other: 1064 nm + 1480 nm) were incorporated into a microfluidic optical stretcher setup. At 1480 nm, the absorption coefficient of water is α = 23.2394 cm^{-1} compared to α = 0.1458 cm^{-1} at 1064 nm.[27] Since the temperature increase in a microfluidic optical stretcher has been measured to be 13–17 °C W^{-1} at 1064 nm[13] and the temperature increase should scale linearly with absorption coefficient ($\Delta T \sim \alpha \cdot P/\Lambda$ where P is the laser power, Λ is the heat conductivity of the medium), we estimate a temperature increase of ΔT(1480) $\approx$ ΔT(1064).(23.2394/0.1458) $\approx$ 2070–2700 °C W^{-1}. We verified the much increased heating at longer wavelengths using COMSOL simulations, which are in agreement with previously published experimental results (see Table 1 and ESI†)

Hence, it is possible with a 1480 nm laser to induce important temperature changes with very small stretching forces. For example, for an applied power of 10 mW at a wavelength of 1480 nm the temperature rise is expected to be about +20 °C whereas the peak stress is about 0.002 Pa, which is thirty times less than the stress applied at 1064 nm for the mere trapping of a vesicle. In addition, the elastic properties of vesicles change drastically below and above the transition temperature T_{m}.[51,52] We then expect an important change in deformation for vesicles below and above T_{m}. To test this, we deformed pure DPPC and DSPC vesicles in a combined 1064–1480 nm optical trap in which the 1480 laser enables us to control the initial temperature and the 1064 nm laser is mainly used to control the optical stress. Transition temperatures for these two phospholipids are T_{m}(DPPC) = 41.6 °C and T_{m}(DSPC) = 55 °C[29] respectively. In this experiment, fiber ends were relatively close ($d_{\mathrm{fiber}} \approx$ 160 μm, see Fig. 1e) which enables a local stretching and heating due to small beam waists (w(1064) $\approx$ 7 μm and w(1480) $\approx$ 7.5 μm). For each step, a constant 1480 nm power is applied to increase the temperature without inducing deformation and then a stretching power at 1064 nm is applied during 2 s.

Typical final deformations when the 1064 nm laser is applied are shown in Fig. 7a. The corresponding major axis deformations are shown in Fig. 7b. Above a given 1064 nm power a local deformation is induced at the center of the vesicle resulting in a final 'lemon shape'. At higher power at 1064 nm, the deformation is then extended to the whole vesicle resulting in a final 'cigar shape'. We also note that during the stretching at 1064 nm, before reaching the final 'cigar shape', the vesicle can exhibit strong deviations from the spheroidal shape as shown in Fig. 7c, especially when the radius R is much bigger than the beam waist w. Such deformations can be rationalized by a rather local heating and stress application, so that the heating-induced softening of the lipid bilayer and the local application of stress lead to such irregular shapes. In general, for these intermediate states and large strains, the cos^2 approximation obviously breaks down. Indeed, the non-trivial coupling
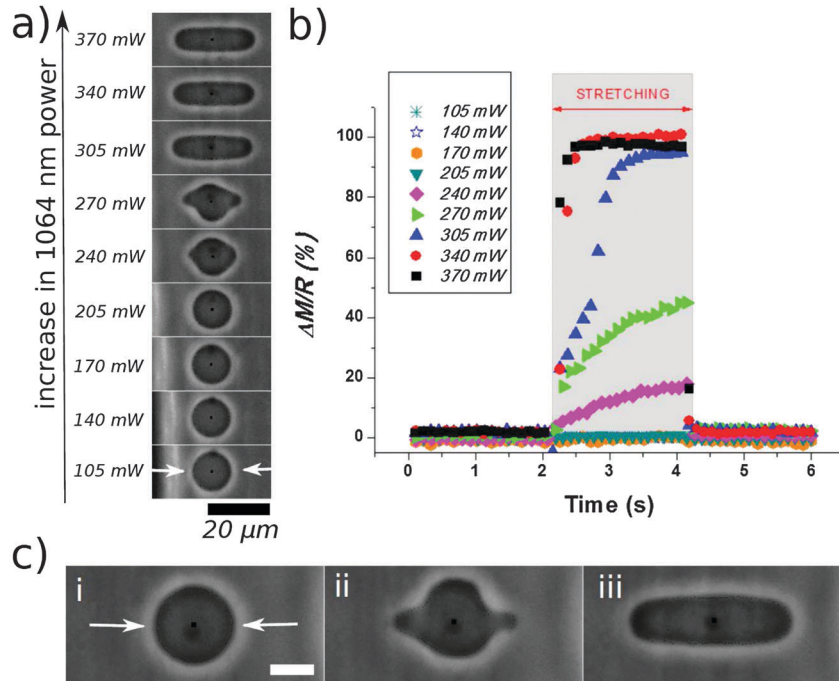

Fig. 7 Deformation pictures (a) and major axis strains (b) of a DPPC vesicle investigated in a double wavelength optical trap with 8 mW at 1480 nm and repeated stretching experiments with increasing powers per fiber at 1064 nm from 105 mW to 370 mW. White arrows indicate laser directions. Black dot indicates the center of the detected vesicle. (c) Dynamic deformation of a DPPC vesicle with 8 mW at 1480 nm and 305 mW at 1064 nm: (i) before stretch (ii) just after the onset of the 1064 nm laser (iii) final shape during the stretch. Scale bar represents 10 μm.

between irregular shape, optically induced stress distributions and heating induced local softening could lead to very interesting but hard to track vesicle shapes. These irregular deformations explain the shapes of the major axis curves at moderate power (240–305 mW) in Fig. 7b. Importantly, Fig. 7b also shows that at high 1064 power (above 340 mW), the major axis strain is constant during the deformation and does not decrease as observed with EPC vesicles at 1064 nm. Similar deformation curves are obtained for DSPC vesicles. The maximum deformation as a function of 1064 nm power applied, but with constant low power at 1480 nm (typically 8–12 mW), is shown in Fig. 8a for DPPC and DSPC vesicles. The major axis strain can be described in terms of three regimes as a function of 1064 nm power: (I) at low 1064 nm power the temperature in the trap is below T_m and the vesicles are in the gel phase. No significant deformation within the uncertainty of the image analysis was detected. (II) When the 1064 nm laser power is above a critical value (≈ 0.2–0.24 W for DPPC and ≈ 0.35–0.4 W for DSPC), the vesicle starts to deform. In this second regime, the deformation increases considerably, which cannot just be attributed to the increase in optically applied stress, but is also due to an increase in the temperature above T_m induced by 1064 nm. The maximum temperature at the center of the trap can be estimated with $T = T_{amb} + 2\beta(1064)\,P(1064) + \beta(1480)\,P(1480)$, where T_{amb} is the ambient temperature, $\beta(\lambda)$ is the coefficient of absorption and $P(\lambda)$ the applied power at the specific wavelength. Thus, at the onset of this second regime, the 1064 nm laser induces only a slight increase in temperature which results in a huge increase in deformation. Since the transition temperature of the DPPC lipid is lower compared to DSPC, the rapid increase in deformation starts at lower 1064 nm powers for DPPC than for DSPC. (III) At higher 1064 nm power the deformation seems to saturate in the range of investigated optical stress. This saturation might be the signature of the saturation regime presented in the theoretical part where all the excess area is stretched. Of note, at these 1480 nm powers, the major axis strain of either DPPC or DSPC vesicles above T_m is considerably larger ($\approx 60\%$ in major axis strain) than for EPC

vesicles ($\approx 30\%$; compare Fig. 3a and 7b). However, such global behaviour of vesicles with a huge increase in deformation clearly shows that the transition temperature can be detected by this double wavelength optical stretcher by converting the thermodynamic transition into a significant deformation. We also analyzed the deformation of vesicles depending on the 1480 nm laser power added to the 1064 nm stretching power. Unfortunately, the vesicles are very sensitive at the transition temperature so lots of them were destroyed by the application of a rapid stretch or a rapid temperature change. Nevertheless, a general deformation diagram is presented in Fig. S5 (see ESI†) for more than thirty vesicles of DPPC and DSPC and typical results are presented in Fig. 8b. For 8 mW at 1480 nm, the expected initial temperature before the application of the 1064 nm laser is around 36 °C. This indicates that DPPC vesicles are in the gel phase at low power in 1064 nm laser and a transition in deformation is observed at higher power. At 21 and 25 mW in 1480 nm, the initial temperature in the trap is expected to be around 60 °C and 70 °C for DPPC, respectively, so the vesicles are in the liquid phase which explains that no transition between regime I–II–III was observed in these cases. Maximum deformation shapes of vesicles for the various 1480 nm power are also shown in Fig. 8b: for 1064 nm investigated here, it clearly appears that the higher the 1480 nm power is, the smaller the final major axis strain is. This behavior might result from the increase in the effective tension with temperature due to an increase of the fluctuations with temperature. To reach the same deformation, a higher optical stress would then be required. However, other parameters such as refractive index involved in the peak stress or volume of the vesicle which both vary with temperature might play a role.

V Discussion

In this work, the deformation of vesicles by various realizations of dual-beam optical traps ("optical stretchers") has been
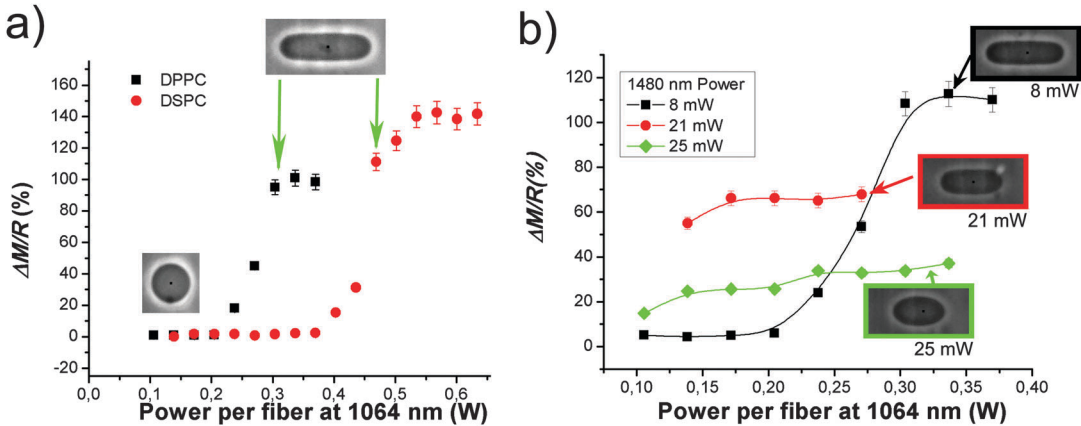

Fig. 8 (a) Major axis strain for DPPC and DSPC vesicles. Green arrows indicate the beginning of a saturation regime. Here the estimated 1480 nm power is $P(1480) = 8$ mW for DPPC and $P(1480) = 11$ mW for DSPC. (b) Deformation of DPPC vesicles depending on the power of the 1480 nm laser. Lines are guides for the eyes. Included are the pictures of the final shape for 8, 21 and 25 mW at 1480 nm. Error bars have been estimated using the maximum and the minimum measured value of $\Delta M/R$ during the deformation.

analyzed experimentally for various laser wavelengths, and models have been proposed to describe the observed deformations. In the absence of heating, a minimal model, which enables the description of the deformation of liquid drops, can be used to roughly rescale our data, which indicates that the total tension remains close to the initial tension. In order to take into account the specific case of the vesicle and extract the bending modulus, we have proposed a more complex approach based on a quasi-spherical approximation. For vesicles, the total tension is dependent on the applied optical stress and the total tension is the associated Lagrangian multiplier to the total surface area. In addition, in our approach, the angular dependence of the stress profile was explicitly considered and approximated by a $\cos^2$ stress profile. This stress profile was used to estimate the initial tension with the liquid drop model and to extract mechanical properties of vesicles (initial tension and bending modulus) with the quasi-spherical model. Interestingly, in the low peak stress regime the $\cos^2$ stress profile approximation seems to be good enough to yield a reasonable estimate of vesicle properties independent of the ratio between vesicle radius and beam waist, R/w, even if this approximation is supposed to correctly fit the optical stress profile for $R/w \approx$ 0.8–0.9. A possible explanation for such a success is presented in Fig. S2 (see ESI†) where the total optical force on an object projected along the fiber axis is calculated with RO approximations and with the $\cos^2$ approximation. Whereas the $\cos^2$ approximation seems to describe correctly the total optical force at small R/w ratios ($0.4 < R/w < 0.9$), some important discrepancies exist at a high R/w ratio ($R/w > 1$). Such discrepancies might be the reason for the underestimation of the bending modulus and for the observed deviation between experiments and the fits (in Fig. 5) for larger vesicles ($R/w =$ 1.44). This trend is also evident from the deviation of the ratio between major and minor axis strain from 2 (which corresponds to volume conservation of spheroid) in the case of large vesicles and high stresses as shown in Fig. 3. These discrepancies are then the likely cause of the scattered data of bending modulus obtained here. To take into account more exact stress profiles, the present theory of vesicle deformation must be extended to other shape modes and experiments must consider the complete shape of the vesicle. This could be done by analyzing the whole shape of the vesicle in Fourier modes and by characterizing the associated spherical harmonics. Regarding the calculation of the stress, GLMT theory has revealed that the optical stress is not zero at the pole ($\theta =$ $\pi/2$),[34] which might also explain the underestimation of the bending modulus. Further developments should include a more realistic angular description of the stress since this residual stress will definitely modify the mechanical equilibrium. Such work is outside the scope of the present study, which however lays the basis for it. The underestimation of the bending modulus could also result from the high sugar concentrations used here as already mentioned in the text. Such high concentrations were used to take full benefit from the laser power to deform vesicles with high optical stresses, especially at 808 nm which was not possible in previous studies. Yet, these concentrations are not required to deform vesicles with optical stretchers provided the laser power is large enough. Currently, high powers are more easily available at 1064 nm with fiber lasers (standard available powers are 5 W). Our study reveals that the choice of the laser wavelength is crucial to avoid any heating effects in the deformation behaviour. Deforming EPC vesicles with a 1064 nm optical stretcher clearly induces a non-steady deformation and a hysteresis in deformation which was not the case with a 808 nm optical stretcher. Such a strain decrease was not observed for pure lipid vesicles. The exact underlying mechanisms of this strain decrease for EPC vesicles are still unknown but the induced temperature by the 1064 nm optical stretcher seems to be at the origin of a reorganization in the membrane, which is composed of several lipids and cholesterol. The 1064 nm optical stretcher has been extensively used to perform deformation studies on biological cells.[17,18,25] Our study shows that these temperature effects might have important consequences for cell rheological measurements using optical stretchers. Two recent studies[53,54] have indeed reported temperature effects for cell rheology and have taken explicit advantage of temperature increases in optical stretchers to perform passive and active thermorheological experiments. Despite the above limitations, characterization of physical properties with an optical stretcher presents significant advantages compared to the standard micropipette technique. Optical stretching enables deformation of vesicles without any physical or chemical contact. This could allow high-throughput characterization of vesicles in microfluidic devices. Compared to optical tweezers, the optical stretcher does not rely on strongly focused laser beams, which avoids laser induced effects such as bilayer buckling for example.[46] One of the most critical aspects of the optical characterization compared to other methods is the absorption of laser which leads to heating and can have dramatic effects by inducing phase transitions. However, this study shows that these heating effects do not need to be detrimental but can be useful to study phase transitions in a dual wavelength optical stretcher.

In conclusion, this work has presented the deformation of vesicles in an optical stretcher. We use an open setup, which enables flexibility, and a microfluidic setup, which can be used for fast characterization of many vesicles. This work validates the use of an 808 nm laser to stretch vesicles at low power as already mentioned in ref. 22, but also at relatively high power, as no significant heating effects have been observed for 808 nm stretching up to 1 W in total power in contrast to the case of 1064 nm stretching. We have proposed a model to account for the observed vesicle deformation and to calculate the elastic properties. A simple model was also proposed for the deformation of liquid drop in the optical stretcher that could be useful for the deformation of drops of very low surface tension, which could help to calibrate the optically induced forces. We have investigated the effect of laser wavelength on the deformation of the vesicles. The decrease of the deformation of a vesicle during a 1064 nm stretching has been described for the first time in the case of a lipid mixture. This effect can safely be attributed to the increased temperature, even if the microscopic mechanism remains to be understood. Eventually, we use a

combined optical stretcher operating at 1064 nm and 1480 nm simultaneously to almost independently apply stress or temperature to the vesicle. We show that it is possible to detect the temperature transition of lipids and to induce strong local curvatures with this combined setup. This work thus lays the basis of a microfluidic integrated tool for the efficient mechanical and thermodynamic characterization of vesicles.

Acknowledgements

References

1 R. Lipowsky and E. Sackmann, *Handbook of biological physics, Structures and Dynamics of membrane*, Elsevier, 2004.

2 U. Seifert, *Adv. Phys.*, 1997, **46**, 13.

3 P. Gill, T. Tohidi Moghadam and B. Ranjbar, *J. Biomol. Tech.*, 2010, **21**, 167.

4 J. Pécreaux, H.-G. Dobereiner, J. Prost, J.-F. Joanny and P. Basserau, *Eur. Phys. J. E: Soft Matter Biol. Phys.*, 2004, **13**, 277.

5 E. Evans and W. Rawicz, *Phys. Rev. Lett.*, 1990, **64**, 2094.

6 K. H. de Haas, C. Blom, D. van den Ende, M. H. G. Duits and J. Mellema, *Phys. Rev. E: Stat. Phys., Plasmas, Fluids, Relat. Interdiscip. Top.*, 1997, **56**, 7132.

7 D. Abreu, M. Levant, V. Steinberg and U. Seifert, *Adv. Colloid Interface Sci.*, 2014, **208**, 129.

8 H. Zhou, B. B. Gabilondo, W. Losert and W. van de Water, *Phys. Rev. E: Stat., Nonlinear, Soft Matter Phys.*, 2011, **83**, 011905.

9 A. T. Brown, J. Kotar and P. Cicuta, *Phys. Rev. E: Stat., Nonlinear, Soft Matter Phys.*, 2011, **84**, 021930.

10 M. Kummrow and W. Helfrich, *Phys. Rev. A: At., Mol., Opt. Phys.*, 1991, **44**, 8356.

11 P. M. Vlahovska, R. S. Gracia, S. Aranda-Espinoza and R. Dimova, *Biophys. J.*, 2009, **96**, 4789.

12 E. J. G. Peterman, F. Gittes and C. F. Schmid, *Biophys. J.*, 2003, **84**, 1308.

13 S. Ebert, K. Travis, B. Lincoln and J. Guck, *Opt. Express*, 2007, **15**, 15493.

14 D. Braun and A. Libchaber, *Phys. Rev. Lett.*, 2002, **89**, 188103.

15 Y. T. Maeda, A. Buguin and A. Libchaber, *Phys. Rev. Lett.*, 2011, **107**, 038301.

16 J. Guck, R. Ananthakrishnan, T. J. Moon, C. C. Cunningham and J. Käs, *Phys. Rev. Lett.*, 2000, **84**, 5451.

17 J. Guck, R. Ananthakrishnan, H. Mahmood, T. J. Moon, C. C. Cunningham and J. Käs, *Biophys. J.*, 2001, **81**, 767.

18 H. K. Matthews, U. Delabre, J. L. Rohn, J. Guck, P. Kunda and B. Baum, *Dev. Cell*, 2012, **23**, 371.

19 F. Lautenschläger, S. Paschke, S. Schinkinger A. Bruel, M. Beil and J. Guck, *Proc. Natl. Acad. Sci. U. S. A.*, 2009, **106**, 15696.

20 K. J. Chalut, M. Höpfler, F. Lautenschläger, L. Boyde, C. J. Chan, A. Ekpenyong, A. Martinez-Arias and J. Guck, *Biophys. J.*, 2012, **103**, 2060.

21 A. E. Ekpenyong, G. Whyte, K. Chalut, S. Pagliara, F. Lautenschläger, C. Fiddler, S. Paschke, U. F. Keyser, E. R. Chilvers and J. Guck, *PLoS One*, 2012, **7**, e45237.

22 M. E. Solmaz, R. Biswas, S. Sankhagowit, J. R. Thompson, C. A. Mejia, N. Malmstadt and M. L. Povinelli, *Biomed. Opt. Express*, 2012, **3**, 2419.

23 M. E. Solmaz, R. Biswas, C. A. Mejia, M. L. Povinellia and N. Malmstadt, *RSC Adv.*, 2013, **3**, 16632.

24 M. Khoury, R. Barnkob, L. Laub Busk, P. Tidemand-Lichtenberg, H. Bruus and K. Berg-Sorensen, *Proc. SPIE*, 2012, **8458**, 84581E.

25 B. Lincoln, F. Wottawah, S. Schinkinger, S. Ebert and J. Guck, *Methods Cell Biol.*, 2007, **83**, 397.

26 J. Guck, R. Ananthakrishnan, C. C. Cunningham and J. Kas, *J. Phys.: Condens. Matter*, 2002, **14**, 4843.

27 K. F. Palmer and D. Williams, *J. Opt. Soc. Am.*, 1974, **64**, 1107.

28 L.-L. Pontani, J. van der Gucht, G. Salbreux, J. Heuvingh, J.-F. Joanny and C. Sykes, *Biophys. J.*, 2009, **96**, 192.

29 C.-H. Lee, W.-C. Lin and J. Wang, *Phys. Rev. E: Stat., Nonlinear, Soft Matter Phys.*, 2001, **64**, 020901(R); E. J. Shimshick and H. M. McConnell, *Biochemistry*, 1973, **12**, 2351.

30 M. Angelova and D. S. Dimitrov, *Prog. Colloid Polym. Sci.*, 1988, **76**, 59.

31 A. E. Ekpenyong, C. L. Posey, J. L. Chaput, A. K. Burkart, M. M. Marquardt, T. J. Smith and M. G. Nichols, *Appl. Opt.*, 2009, **48**, 6344.

32 P. B. Bareil, Y. Sheng and A. Chiou, *Opt. Express*, 2006, **14**, 12503.

33 L. Boyde, K. J. Chalut and J. Guck, *J. Opt. Soc. Am. A*, 2009, **26**, 1814.

34 L. Boyde, A. E. Ekpenyong, G. Whyte and J. Guck, *Appl. Opt.*, 2012, **51**, 7934.

35 F. Xu, J. A. Lock, G. Gouesbet and C. Tropea, *Phys. Rev. A: At., Mol., Opt. Phys.*, 2009, **79**, 053808.

36 H. C. van de Hulst, *Light scattering by small particles*, Dover, 1981.

37 F. Wottawah, S. Schinkinger, B. Lincoln, R. Ananthakrishnan, M. Romeyke, J. Guck and J. Kas, *Phys. Rev. Lett.*, 2005, **94**, 098103.

38 R. Ananthakrishnan, J. Guck, F. Wottawah, S. Schinkinger, B. Lincoln, M. Romeyke, T. Moon and J. Kas, *J. Theor. Biol.*, 2006, **242**, 502.

39 F. Brochard, P. G. De Gennes and P. Pfeuty, *J. Phys.*, 1976, **37**, 1099.

40 P. C. F. Møller and L. B. Oddershede, *Europhys. Lett.*, 2009, **88**, 48005.

41 U. Seifert, *Eur. Phys. J. B*, 1999, **8**, 405.

42 U. Seifert, *Z. Phys. B: Condens. Matter*, 1995, **97**, 299–309.

43 V. Vitkova, J. Genova and I. Bivas, *Eur. Biophys. J.*, 2004, **33**, 706.

44 M. B. Sankaram and T. E. Thompson, *Proc. Natl. Acad. Sci. U. S. A.*, 1991, **88**, 8686.

45 J. H. Ipsen, O. G. Mouritsen and M. J. Zuckermann, *Biophys. J.*, 1989, **56**, 661.

46 R. Bar-Ziv, E. Moses and P. Nelson, *Biophys. J.*, 1998, **75**, 294.

47 R. M. Servuss, W. Harbich and W. Helfrich, *Biochim. Biophys. Acta*, 1976, **434**, 900.

48 J. F. Faucon, M. D. Mitov, P. Méléard, I. Bivas and P. Bothorel, *J. Phys.*, 1989, **50**, 2389.

49 M. Murrell, L. L. Pontani, K. Guevorkian, D. Cuvelier, P. Nassoy and C. Sykes, *Biophys. J.*, 2011, **100**, 1400.

50 J. Genova, A. Zheliaskova and M. D. Mitov, *Colloids Surf., A*, 2006, **282**, 420.

51 L. Fernandez-Puente, I. Bivas, M. D. Mitov and P. Méléard, *Europhys. Lett.*, 1994, **28**, 181.

52 C.-H. Lee, W.-C. Lin and J. Wang, *Phys. Rev. E: Stat., Nonlinear, Soft Matter Phys.*, 2001, **64**, 020901R.

53 T. R. Kiessling, R. Stange, J. A. Käs and A. W. Fritsch, *New J. Phys.*, 2013, **15**, 045026.

54 C. J. Chan, G. Whyte, L. Boyde, G. Salbreux and J. Guck, *Interface Focus*, 2014, **4**, 20130069.